Electronic Supplementary Material (ESI) for Physical Chemistry Chemical Physics.

Electronic Supplementary Information

Electrochemical Cell Design Parameters for Quantitative Evaluation of CO_2 Reduction Electrocatalysts

Peter Lobaccaro,[abc] Meenesh Singh,[abc] Ezra Lee Clark,[abc] Youngkook Kwon,[ac] Alexis T. Bell,*[abc] and Joel W. Ager*[ade]

[a.] *Joint Center for Artificial Photosynthesis, Lawrence Berkeley National Laboratory, CA 94720, USA. E-mail: alexbell@berkeley.edu; jwager@lbl.gov*
[b.] *Chemical Sciences Division, Lawrence Berkeley National Laboratory, CA 94720, USA.*
[c.] *Department of Chemical and Biomolecular Engineering, University of California, Berkeley, CA 94720, USA.*
[d.] *Materials Sciences Division, Lawrence Berkeley National Laboratory, CA 94720, USA.*
[e.] *Department of Materials Science and Engineering, University of California, Berkeley, CA 94720, USA.*

Table of Contents

Description of Electrochemical Cells Reported for CO2RR

The design parameters of CO2R reaction cells used in a number of literature reports are tabulated. Shading is used to indicate designs with electrode surface area to electrolyte volume (*S/V*) ratios of greater than 0.5. In those cells, based on the results of this study, depletion of CO_2 could conceivably be a concern depending on the current and CO_2 sparging method used.

Report	Design	Cathode *S/V* Ratio (cm^{-1})	Comments
Hori *et al.*, 1989.[1]	H-Cell, 3 compartment cell, gas flow	8/60 = 0.133	A temperature control bath was used. In the 3-compartment design, 2 counter electrodes were used, one for each face of the working electrode foil.
Azuma *et al.*, 1990.[2]	H-Cell, gas flow	Not given	No bulk electrolyte pH reported.
Köleli *et al.*, 2003.[3]	Fixed-Bed reactor, gas flow	148-345/100 = 1.48-3.45	mm-sized-bead catalysts used. First attempt to use a fixed bed reactor to do electrochemical CO2R. No bulk electrolyte pH reported.
Li *et al*., 2005.[4]	Sandwich style, gas & liquid flow	Not Given	First application of sandwich style flow cell. Gaseous CO_2 flown concurrently with saturated carbonate electrolyte.
Kuhl *et al.,* 2012.[5]	Sandwich style, gas flow	4.5/8 = 0.56	High ratio of catalyst area to electrolyte volume enabled detection of C_2^+ products by NMR. No bulk electrolyte pH reported.
Li *et al.*, 2012.[6]	H-Cell, gas flow	2/20 = 0.1	Larger volume cell, similar to Azuma *et al.* The large volume mitigates mass transfer limitations. No bulk electrolyte pH reported.
Lu *et al.*, 2014.[7]	H-Cell, no gas flow	(0.25-1)/80 = 0.003-0.01	Reactor was initially charged with CO_2 and sealed. Mass transfer enhanced with magnetic stirring. No bulk electrolyte pH reported.
Kim *et al.*, 2014.[8]	Sandwich style, gas flow	1.1/33 = 0.033	No bulk electrolyte pH reported.
Manthiram *et al.*,2014.[9]	Sandwich style, gas flow	5.2/5 = 1.04	Single bubble sparger used. No bulk electrolyte pH reported.
Li *et al*., 2014.[10]	Same as Li *et al.*, 2012	2/20 = 0.1	Same as Li *et al.*, 2012
Sen *et al*., 2014.[11]	H-Cell, gas flow	Not Given	No bulk electrolyte pH reported.
Kas *et al*., 2015.[12]	Pressure Cell, similar to H-Cell, gas flow	Not Given	No bulk electrolyte pH reported.
Ma *et al.*, 2015.[13]	Sandwich style, gas flow	Not Given	No bulk electrolyte pH reported.
Clark *et al*., 2015.[14]	Sandwich style, liquid flow	1/0.025 = 40	External saturation of CO_2 is used. No bulk electrolyte pH reported for electrolyte exiting cell.
Kortlever *et al*., 2015[15]	H-Cell, gas flow	Not Given	No bulk electrolyte pH reported.
This work	Sandwich style, gas flow	1/0.5-1.5 = 2-0.67	*In-situ* probing of pH and temperature to measure CO_2 concentration in the electrolyte

Electrochemical Cell Design Details

The smaller cell A was designed to create the maximum surface area to volume ratio possible with the sandwich geometry while still incorporating replaceable bubblers and gas tight fittings. Each compartment of this cell was machined out of a piece of polycarbonate (2 in. × 2 in. × 0.22 in.) which is quite chemically resistant while still being relatively easy to machine. Polycarbonate has the added benefit of being transparent so that the interior of the cell can be monitored. The reaction chamber contains 0.5 mL of electrolyte and has 0.33 mL of headspace. All tubing and fittings used with the cell were purchased from IDEX Health and Science. A 360 µm OD, 150 µm ID PFA HP Plus tube was used as the bubbler with a PFA 360 µm ID, 1/16" OD tubing sleeve. 1/16" OD PFA HP Plus tubing was connected to the outlet of the cathode compartment. IDEX M-6-40 PEEK flat bottom port super flangeless fittings were used to connect the tubing to the cell.

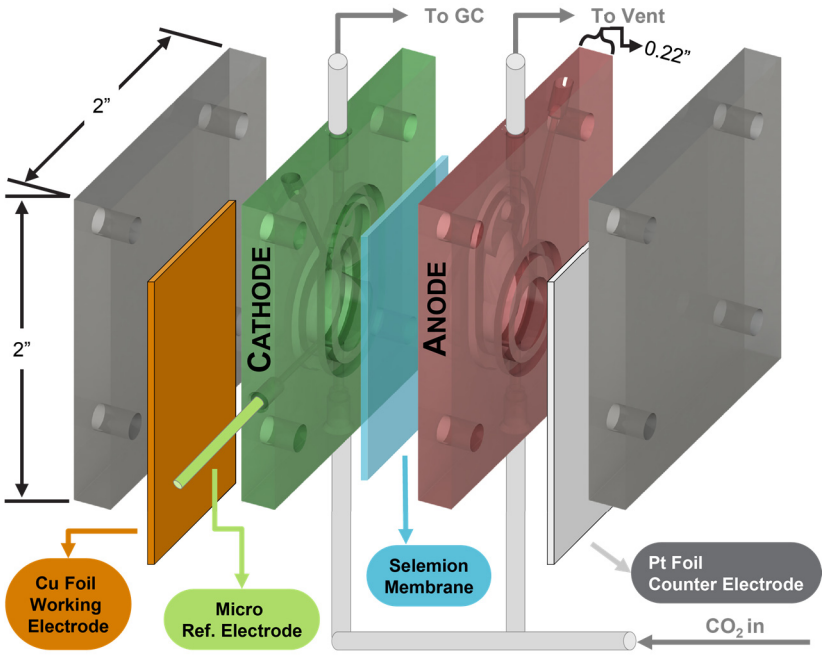

Fig. S1 CO2R Electrochemical Cell Design: Cell A with the smaller electrolyte volume is pictured here, a schematic of Cell B is Fig. 1 of the main text. The cell is made up of 2 polycarbonate compartments with identical volumes separated by a membrane. Both sides are sparged with CO_2 using a capillary tube and the gaseous products produced at the Cu cathode are swept away to be analyzed by GC.

The larger cell B (Fig. 1) was designed to be the smallest design possible in which a removable glass frit bubbler could be installed in the cell to reduce the size of the sparging CO_2 bubbles (installing a removable frit in the small cell was not possible). Each compartment of this cell was machined out of a piece of polycarbonate (2 in. ×2.2 in. × 0.48 in.). The reaction chamber

contains 1.5 mL of electrolyte and has 0.75 mL of headspace. The bubbling assembly was composed of an 6 mm OD P4 thimble frit fused onto a 1/8" glass down tube (Adams & Chittenden Glass) and a 1/8" Male NPT to 1/8" Swagelok compression bored-through fitting made of nylon (Swagelok). The glass tube was inserted through the Swagelok fitting and then screwed into the bottom of the cell to make a seal. The NPT side sealed the fitting into the cell and the Swagelok side sealed the frit assembly into the fitting there by sealing the combination to liquid and gas leaks. A 1/8" to 1/16" Swagelok reducing union made of nylon (Swagelok) was used to connect the glass tube to the gas supply system. 1/16" OD PFA HP Plus tubing (IDEX) was connected to the outlet of the cell with an IDEX ¼-28 PEEK flat bottom port super flangeless fitting.

CAD drawings of these cells have been uploaded separately.

Liquid Product Detection Limits as a Function of *S/V*

The use of high *S/V* electrochemical cells will facilitate detection of liquid products. As an example, we consider a hypothetical catalyst which has a 5% faradaic efficiency for producing ethanol (12 e^-/mol) at 5 mA/cm^2. The amount of time required for ethanol to accumulate to 1 mM (a typical detection limit for HPLC or NMR) in the solution can be related to the *S/V* ratio of the cell as follows:

$$\text{Time [min]} = \frac{C_x\, n_x\, F}{S/_V\; FE_x\, J\; 60{,}000} \tag{S1}$$

where C_x is the concentration of the target analyte x in mM, n_x is the number of electrons required per reaction to produce compound x, F is Faraday's constant (96485.3 C/mol), *S/V* is the surface area to volume ratio of the electrochemical cell in cm^{-1}, FE_x is the partial faradaic efficiency to produce product x, and J is the current density in mA cm^{-2}. Figure S2 graphs the required time to reach the detection limit vs. *S/V*. For this example, a cell *S/V* ratio of >1 cm^{-1} will be required to detect ethanol within one hour of cell operation.

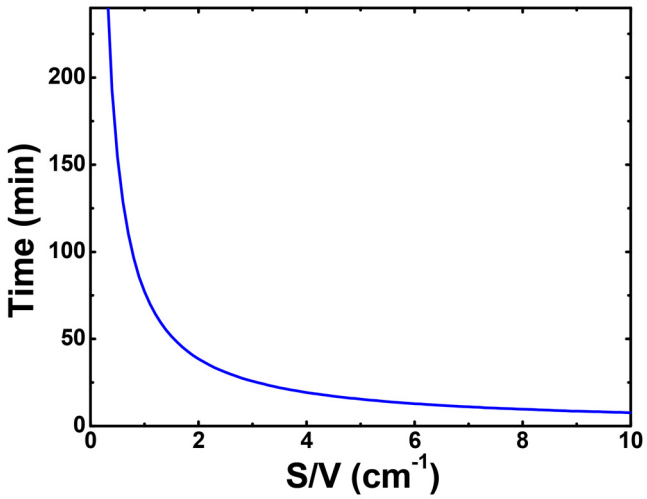

Fig. S2 *S/V* Ratio Effect on Detection Speed: Time required to detect ethanol at a detection limit of 1 mM for a hypothetical CO2R catalyst producing ethanol at 5% faradaic efficiency at 5 mA cm^{-2} graphed as a function of the electrode surface to electrolyte volume ratio *S/V*.

Analysis of Gaseous Products

4.5 LS grade CO_2 (Praxair) was used as the reactant gas. This gas was further purified using a CO_2 gas purifier (Vici) to bring the gas purity above 6.0. The gas flow rate into the cell was controlled with an Alicat Scientific mass flow controller which has a control range of 0.5-100 sccm. The gas flow rate out of the cell was monitored with an Alicat Scientific mass flow meter to ensure there were no gas leaks. Gas was continuously sparged through the electrochemical cell at 5 sccm and then through 2 sampling loops of a SRI multigas #3 EPC gas chromatogram. The GC is equipped with two separate channels. Channel 1 contains a 6' Heysep-D and a 6' Molsieve 13x column, a 1 ml sampling loop, and uses He carrier gas. It is equipped with a thermal conductivity detector (TCD) and a flame ionization detector (FID) with a methanizer attachment for the conversion of CO to CH_4. The quantitative detection limits for this channel are 2 ppm for CH_4, CO, and C_2H_4. Ethane (C_2H_6) can also be detected on this channel but was not observed in any experiments performed in this study. Channel 2 contains a 6' Heysep-D column, a 2 ml sampling loop, and N_2 carrier gas. It is equipped with a TCD detector and has a quantitative detection limit of 100 ppm for H_2. N_2, He, and H_2 gases supplied to the GC were 5.0 ultra-high purity grade (Praxair) and each passed through its respective gas purifier (Vici) to bring the gas purity up to 6.0.

The GC method developed here eluted the relevant gases in ~ 13 minutes (Fig. S3). The next step in the cycle was a bake, performed after every injection, to insure all water vapor was removed from the columns before the next injection. The CO_2 gas is not observed due to the use of a bypass valve which was activated to divert the CO_2 to around the FID detector. Gas flowing from the electrochemical cell was sampled every 20 minutes.

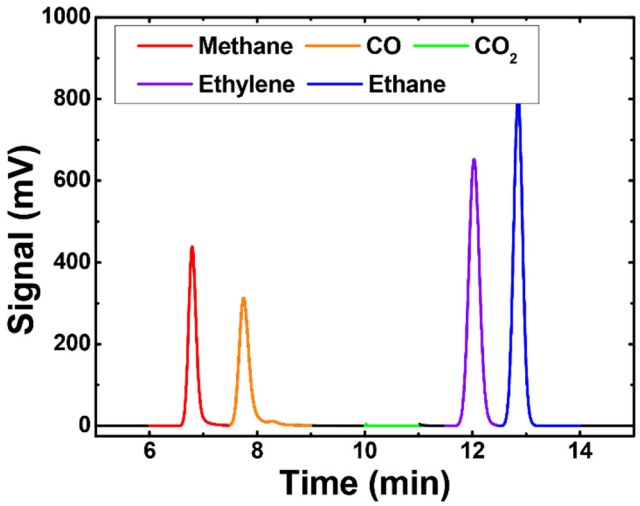

Fig. S3 GC FID Product Detection: 1000 ppm standards of expected gaseous products of CO_2 were injected together to produce the chromatogram. The area where the CO_2 purge gas would elute is highlighted in green; a bypass valve was used to isolate this gas from the detector. Good separation is achieved between all 4 of the major gaseous products.

Analysis of Liquid Products

The liquid products were collected from the cathode and anode chambers after electrolysis and analyzed by high-pressure liquid chromatography (HPLC) on an UltiMate 3000 (Thermo Scientific). The column used was an Aminex HPX 87-H (Bio-Rad) with a dilute sulfuric acid (1 mM) eluent. The column was maintained at 60°C in a column oven, and the effluent from the column was passed through a refractive index detector (RID) to identify compounds of interest. Vials with the collected samples were placed in a chilled autosampler holder and 10 µL of sample was injected onto the column. In order to quantitatively identify the constituents in the sample, a standard calibration curve was generated for the expected products of CO2R (e.g. formate, acetate, acetaldehyde, ethanol, propionaldehyde, 1-propanol) as shown in Fig. S4.

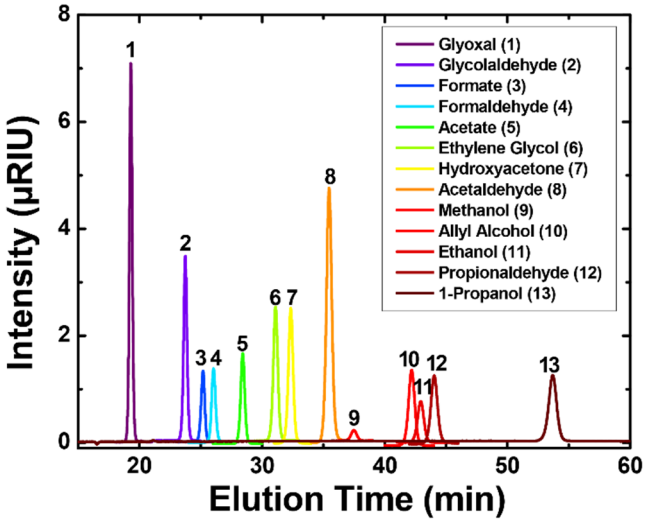

Fig. S4 HPLC Liquid Product Detection: A chromatograph shows the ability to separate all 13 liquid products of interest for CO2R. 10 mM standards of each compound were injected sequentially and their traces overlaid to produce this plot.

A control experiment was performed to experimentally verify the improved detection limit for liquid products in the cell with the larger *S/V* ratio, cell A. Cu foil was used as the cathode and in order to reduce any possible mass transfer effects on this experiment the cells were operated at ~ -0.95V vs. RHE where the current densities are lower, ~ 4.45 mA cm^{-2}. At this potential, only small amounts of liquid products are expected to be generated. Also, to show the speed with which liquid products can be accumulated in these cells, the run time was reduced to only 30 minutes after which time the liquid was extracted from the anode and cathode chambers of each cell. We re-emphasize that the liquid needed to be extracted from both chambers because negatively charged liquid CO2R products, like acetate and formate, can cross over the selemion membrane from the cathode chamber to the anode chamber. The concentrations of liquid products of the two chambers were then added together for the final analysis.

During the experiments, similar amounts of charge were passed and the faradaic efficiencies for formate, the only detected liquid product, were comparable (Table S1). As expected, Cell A, which has a higher *S/V* ratio, showed a higher total signal than Cell B and both were comfortably within the detection limit of the HPLC (~ 0.1 mM). The approximate doubling in the concentration of formate detected per charge passed from Cell A to Cell B was expected as a result of the difference in *S/V* between the two cells.

Table S1: Summary of results of formate detection in the electrolyte of Cell A and Cell B after performing commensurate CO2R experiments. Cu foil was used as the cathode in 0.1 M $NaHCO_3$ with CO_2 sparging at 5 sccm at 1 atmosphere.

Conditions (units)	Cell A	Cell B
Applied Voltage (V vs. RHE)	-0.933	-0.963
Current Density (mA/cm^2)	4.59	4.32
Run Time (min)	30	30
Charge Passed (C)	8.35	7.76
$FE_{Formate}$ (%)	2.8	4.3
Peak Area [Formate] (Arb.)	0.094	0.041
Concentration (mM)	1.985	0.869
Concentration/Charge Passed (mM/C)	0.24	0.11

Equilibrium Equations for CO_2/Carbonate/Bicarbonate Family

For this detailed discussion of the CO_2/carbonate/bicarbonate equilibria, Eqs. (1)-(4) of the main text, are reproduced here as (S2)-(S5).

$$CO_{2(g)} \rightleftharpoons CO_{2(aq)} \tag{S2}$$

$$CO_{2(aq)} + H_2O \rightleftharpoons H^+ + HCO_3^- \tag{S3}$$

$$HCO_3^- \rightleftharpoons H^+ + CO_3^{-2} \tag{S4}$$

$$H_2O \rightleftharpoons H^+ + OH^- \tag{S5}$$

Equilibrium constants for reactions (S2)-(S5) are as follows:

$$K_0 = \frac{[CO_{2(aq)}]}{[CO_{2(g)}]} = \frac{[CO_{2(aq)}]}{[f_{CO_2}]} \tag{S6}$$

$$K_1 = \frac{[H^+][HCO_3^-]}{[CO_{2(aq)}]} \tag{S7}$$

$$K_2 = \frac{[H^+][CO_3^{-2}]}{[HCO_3^-]} \tag{S8}$$

$$K_w = [H^+][OH^-] \tag{S9}$$

K_0, the Henry's Law coefficient, and the equilibrium constants K_1, K_2, and K_w all depend on temperature and, to some extent, on the composition of the electrolyte. The solubility of a gas in a salt solution (C_G) relative to that in pure water ($C_{G,0}$) is expressed by the Sechenov equation:[16–18]

$$\log\left(\frac{C_{G,0}}{C_G}\right) = K_s\, C_s\,, \tag{S10}$$

where K_s is the Sechenov constant and C_s is the concentration of the salt solution. Using data from 22 gases with 24 cations and 26 anions, Weisenberger and Schumpe found that the Sechenov constant could be fit with the following equation:[18]

$$K_s = \Sigma(h_i + h_G) \tag{S11}$$

where h_i is an ion dependent model fitting parameter and h_G is the gas dependent model fitting parameter. h_G is further dependent on temperature:

$$h_G = h_{G,0} + h_T(T - 298.15\ \text{K}) \tag{S12}$$

where T is the temperature of the solution of interest in Kelvin, h_T is the temperature dependent model fitting parameter, and $h_{G,0}$ is the fitting parameter for the reference state at 298.15 K. There is extensive literature on the solubility of gases (O_2, CO_2, N_2O, etc.) in aqueous salt solutions and this general approach

has been shown to effectively replicate experimental data for a wide range of gases and salt solutions. Although a direct measurement of the CO_2 solubility in bicarbonate buffer could not be found, the Schumpe parameters for Na^+ and HCO_3^- can be used to estimate the "salting out" effect expected here for 0.1 M solution at 25°C. A sample calculation is shown below (Table S2, S3, Eq S13, S14)

Table S3: Ion Dependent Schumpe Model Parameters

Ion	h_i **[M]**
Na^+	0.1143
HCO_3^-	0.0967

Table S2: Gas Dependent Schumpe Model Parameters

Gas	$h_{G,0}$ **[M]**	h_T **[M k^{-1}]**
CO_2	-1.72E-02	-3.38E-04

$$h_G = -0.0172 - 3.38 * 10^{-4} * (298 - 298.15) = -0.01715 \tag{S13}$$

$$\begin{aligned} \log\left(\frac{C_{G,0}}{C_G}\right) &= 0.1 * (0.1143 - 0.01715) \qquad [Na^+] \\ &+ 0.1 * (0.0967 - 0.01715) \qquad [HCO_3^-] \\ &= 0.1767 \end{aligned} \tag{S14}$$

At 25°C C_G is 96.5% of $C_{G,0}$ and over the entire temperature range of 10°C to 40°C C_G is 96.3% to 96.7% of $G_{G,0}$.

It is furthermore known that K_1 and K_2 depend on the salt concentration in aqueous solution from marine chemistry.[19] The following equations, derived from field measurements, describe the changes found for the range of salinity S (5-40, in parts per thousand by mass) and temperature (0-40°C) found in sea water:

$$\log(K_1) = -\frac{3633.86}{T} + 60.88998 - 9.6777 * \ln(T) + 0.011555 * S - 0.0001152 * S^2 \tag{S15}$$

$$\log(K_2) = -\frac{471.78}{T} - 26.94623 + 3.16937 * \ln(T) + 0.01781 * S - 0.0001122 * S^2 \tag{S16}$$

where T is the temperature in Kelvin. It should be noted that these equations do not apply to arbitrary salt solutions, as do the Schumpe relationships for Henry's constant. Nevertheless, it is possible to estimate the effect of salt concentration on K_1 and K_2 using this empirical data. A comparison was made between the values given by Eq. S15-S16 when the salinity of our solution (being the weight of the sodium ions in solution) was used as compared to when the salinity was set to zero. It was found that for K_1 and K_2 the difference was less than 10%.

The results of this analysis led us to use data for pure water for K_0, K_1, K_2, and K_w The Henry's constant (Mol L^{-1}) and equilibrium constants K_1 (Mol L^{-1}) and K_2 (Mol L^{-1}) were taken from the comprehensive review of Plummer *et al.*[20]

$$\log(K_0) = 108.3865 + 0.01985076 * T - \frac{6919.53}{T} - 40.4515 * \log(T) + \frac{669365}{T^2} \tag{S17}$$

$$\log(K_1) = -356.3094 - 0.06091964 * T + \frac{21834.37}{T} + 126.8339 * \log(T) - \frac{1684915}{T^2} \quad \text{(S18)}$$

$$\log(K_2) = -107.8871 - 0.03252849 * T + \frac{5151.79}{T} + 38.9256 * \log(T) - \frac{563713.9}{T^2} \quad \text{(S19)}$$

The water dissociation constant (K_w) was taken from Bandura *et al*.[21]

$$\log(K_w) = 12 * \left(\log(1+Z) - \frac{Z}{Z+1} * D_{H_2O} * \left(0.642044 - \frac{56.8534}{T} - 0.375754 * D_{H_2O} \right) \right) \quad \text{(S20)}$$
$$+ pK_w^G + 2 * \text{Log}\left(\frac{M_w}{1000}\right)$$

$$Z = D_{H_2O} * \exp\left(-0.864671 + \frac{8659.19}{T} - \frac{22786.2}{T^2} * \left(D_{H_2O}\right)^{\frac{2}{3}} \right) \quad \text{(S21)}$$

$$pK_w^G = 0.61425 + \frac{48251.33}{T} - \frac{67707.93}{T^2} + \frac{10102100}{T^3} \quad \text{(S22)}$$

T is in the units of Kelvin throughout Eq. S17-S22. Furthermore, for the water dissociation constant, which is dependent on the density of water (D_{H_2O}), a constant density of 1 g/cm^3 was used. Figure S5 shows the results of solving equations S6-S9 and S17-S22 as a function of temperature for a 0.1 M $NaHCO_3$ buffer solution in equilibrium with 1 atm of CO_2. As discussed in the main text, using the pure water formulas here, the pH of 0.1M $NaHCO_3$ in equilibrium with 1 atm of CO_2 was found to be 6.82. This was then experimentally confirmed, supporting the decision to use the pure water thermodynamic equations.

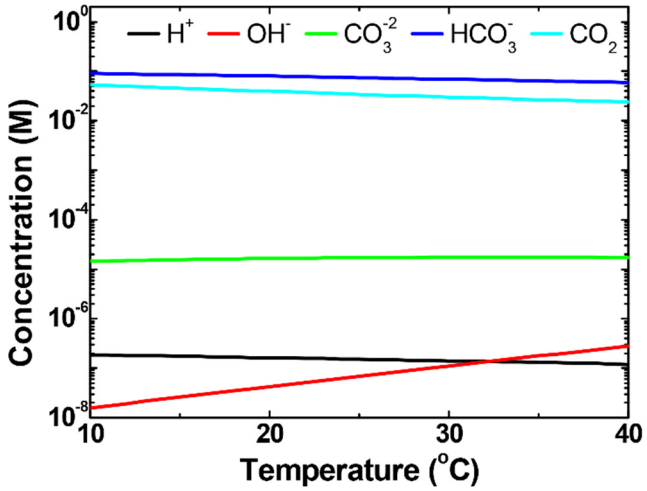

Fig. S5 Equilibrium Electrolyte Species Conc. Vs. Temp: By solving Eqs. S6-S9, the equilibrium concentrations of the ionic species and the dissolved CO_2 was obtained for a 0.1 M $NaCO_3$ buffer solution in equilibrium with 1 atm of CO_2.

Photographs of Cells during Operation

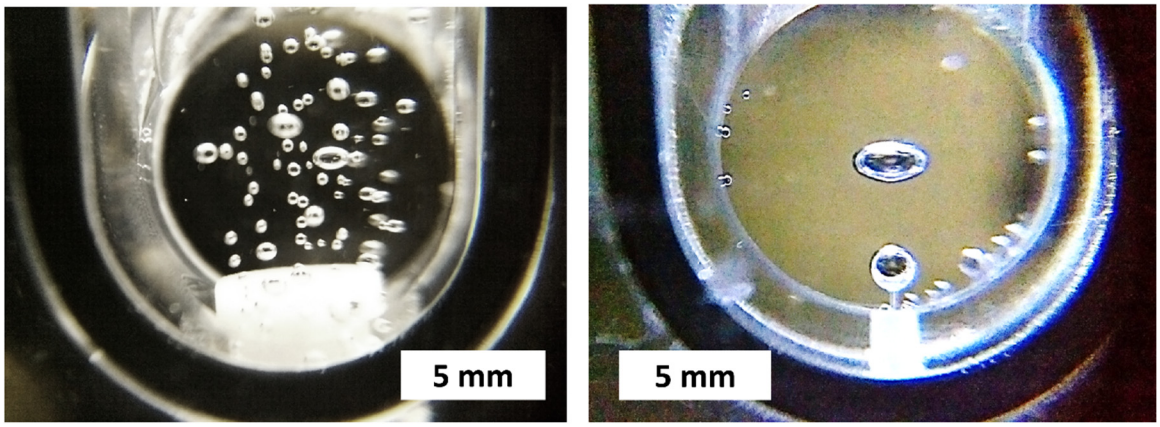

Fig. S6 Images of CO_2 Sparging Bubbles: On the left, bubbles characteristic of those produced by the glass frit are shown. The bubbles have an average radius of ~0.19 mm. On the right, bubbles characteristic of those produced by the single bubbler are shown. These bubbles have an average radius of ~1.2 mm. In both cases a flow rate of 5 sccm of CO_2 was used. Bubble area was calculated using image processing through ImageJ. This area was then converted to an effective spherical bubble radius, assuming the area measured with ImageJ was for a circle which was the center cross-section of a sphere.

Gaseous Products of CO2R on Cu Foil

Figure S7 and Tables S4 and S5 summarize the faradaic efficiencies for gaseous products (CH_4, CO, H_2, C_2H_4) produced by electropolished copper foil at -1.05 V vs. RHE in 0.1 M $NaHCO_3$. Data from Cell A and Cell B are compared. Clearly, H_2 generation dominates in the smaller Cell A ($S/V = 2$) compared to the larger cell, where CH_4 is the dominant product. This effect is due to depletion of CO_2 in the small cell, as discussed in the main text. It can also be seen that both product distributions are quite stable over time except for ethylene production in Cell B. It is still unclear at this time what is causing the decrease in partial faradaic efficiency for this product; however, it is commonly observed in our experiments. It could possibly be due to in-situ surface rearrangement of the polycrystalline Cu surface which is known to happen over time.[22]

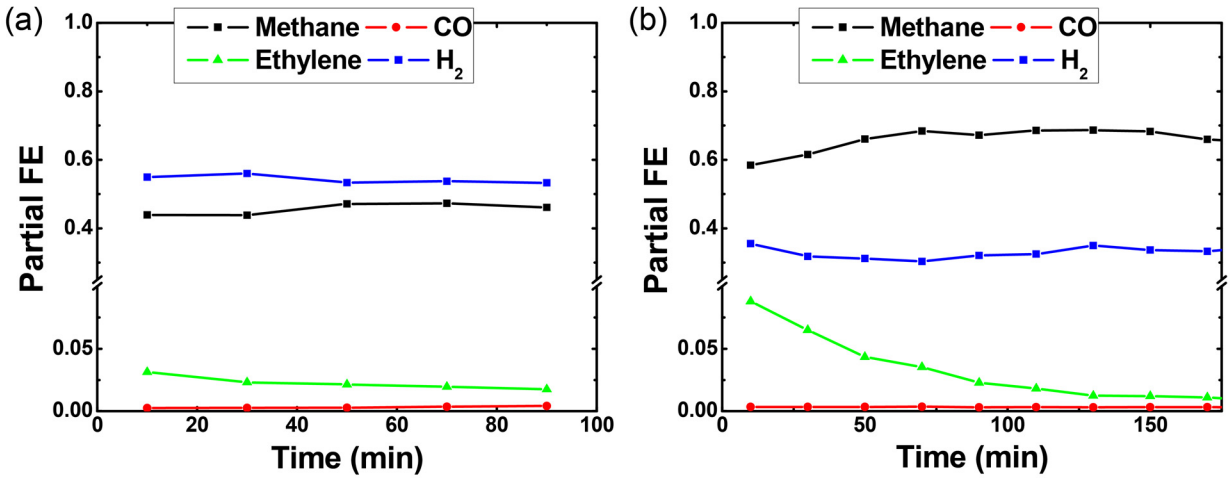

Fig. S7 Gaseous Products of CO2R Vs. Time: Characteristic data of the gaseous products of CO2R at -1.05 V vs. RHE on Cu foil in 0.1M $NaHCO_3$ is plotted here over the course of a 1.5 hr run in Cell A (a) and a 3hr run in Cell B (b)

Table S4: Tabulated current and faradaic efficiency data for CO2R experiment in Cell A at ~ -1.05 V vs. RHE on Cu foil in 0.1M $NaHCO_3$

Time (min)	Current Density (mA/cm^2)	Methane	Carbon Monoxide	Ethylene	Hydrogen	Sum
10	12.40	43.88	0.25	3.13	54.90	102.16
30	12.25	43.82	0.26	2.31	56.02	102.41
50	11.86	47.10	0.28	2.15	53.32	102.85
70	11.66	47.29	0.35	1.96	53.75	103.35
90	11.35	46.10	0.41	1.75	53.30	101.56
Average	11.90	45.64	0.31	2.26	54.26	102.46
Standard Dev	0.43	1.69	0.07	0.53	1.18	0.68

Table S5: Tabulated current and Faradaic efficiency data for CO2R experiment in Cell B at ~ -1.05 V vs. RHE on Cu foil in 0.1M $NaHCO_3$

Time (min)	Current Density (mA/cm^2)	Methane	Carbon Monoxide	Ethylene	Hydrogen	Sum
10	11.86	58.40	0.34	8.80	35.54	103.07
30	11.94	61.56	0.34	6.50	31.76	100.16
50	11.45	66.08	0.34	4.34	31.15	101.91
70	11.04	68.37	0.35	3.53	30.34	102.59
90	10.94	67.20	0.31	2.29	32.09	101.89
110	10.75	68.56	0.33	1.81	32.49	103.18
130	10.52	68.65	0.31	1.25	34.94	105.14
150	10.41	68.24	0.33	1.22	33.65	103.44
170	10.23	65.96	0.33	1.10	33.25	100.63
190	9.88	65.02	0.28	0.80	34.69	100.79
Average	10.90	65.80	0.33	3.16	32.99	102.28
Standard Dev	0.68	3.39	0.02	2.67	1.72	1.52

Modeling of Electrode Boundary Layer

The effect of changes in the bulk CO_2 concentration on the concentration of CO_2 and the pH at the surface of the electrode was modeled by solving the reaction-diffusion equations for CO_2, HCO_3^-, CO_3^{-2}, and OH^- in the boundary layer (H^+ and OH^- were assumed in equilibrium). Although more sophisticated models have been developed,[23] we used the simple 1D model developed by Gupta *et al.*[24] as it captures the essential phenomena and has been used recently in the literature for similar analyses.[12] The equilibrium constants for reactions (S2)-(S5) used were the same as those discussed above and the forward and reverse reaction rate constants for (S3) and (S4), as well as the diffusion coefficients for CO_2, HCO_3^-, CO_3^{-2}, and OH^- were taken from the recent modeling study of Singh *et al.*[23] It was assumed that electro-neutrality applies and a boundary layer thickness of 100 μm was also assumed. The experimentally measured pH was used to calculate the concentrations of CO_2, HCO_3^-, CO_3^{-2} in the bulk, which was used as the boundary condition at the border between the bulk and the boundary layer. The two extreme cases were modelled; Cell A with a bulk pH of 6.92, the value being elevated as compared to the initial saturated value of 6.7 due to inadequate gas-liquid mass transfer, and Cell B with a bulk pH of 6.78. The experimentally measured current density and product distribution were applied as the boundary conditions at the electrode surface (see Fig S7). The results of this calculation are shown in Figure S8 and Table S6 and S7. While there is only a small decrease in pH for cell A compared to cell B, the effect on the predicted surface concentration of CO_2 is substantial, with a 20% lower concentration for cell A. We note that an even lower concentration would have been predicted if CO_2 reduction current density were higher; clearly, the reduction in bulk pH translates into reductions in the surface CO_2 concentration, which in turn affects the product distribution.

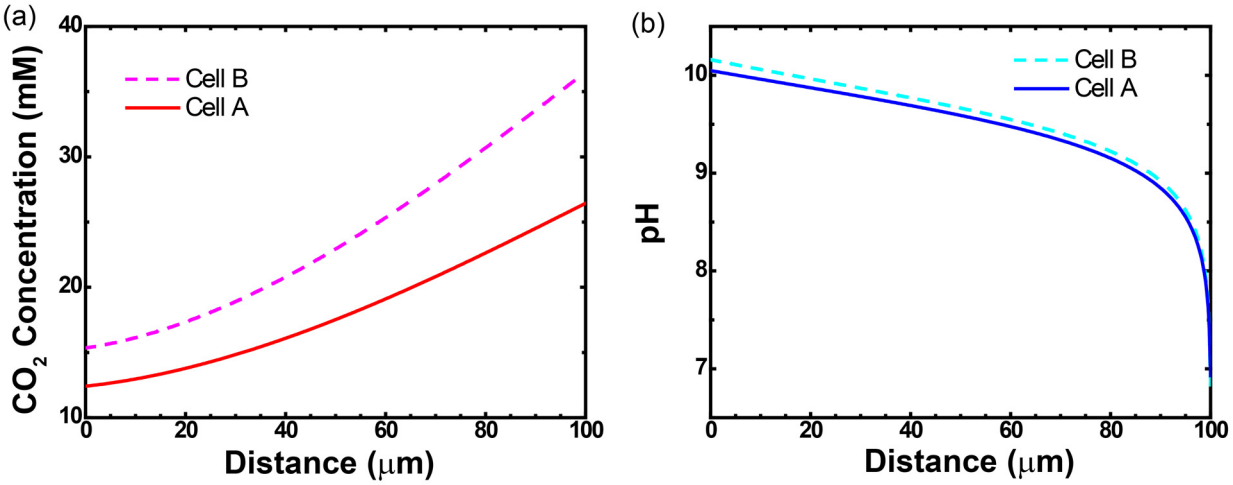

Fig. S8 Boundary Layer Depletion: The concentration profile of CO_2 (a) and pH profile (b) in the boundary layer are shown for the two extreme cases of Cell A and Cell B. The inadequate gas-liquid transfer in Cell A leads to a lower surface concentration of CO_2 and a slightly lower surface pH.

Table S6: Tabulated bulk and surface conditions obtained by 1D modeling for the CO2R experiment in Cell A at ~ -1.05 V vs. RHE on Cu foil in 0.1M $NaHCO_3$

Component	**Bulk Condition**	**Surface Condition**
CO_2	26.44 mM	12.41 mM
HCO_3^{-1}	99.92 mM	82.51 mM
CO_3^{-2}	0.04 mM	43.09 mM
OH^-	8.98 x10^{-5} mM	0.12 mM
pH	6.93	10.05

Table S7: Tabulated bulk and surface conditions obtained by 1D modeling for the CO2R experiment in Cell B at ~ -1.05 V vs. RHE on Cu foil in 0.1M $NaHCO_3$

Component	**Bulk Conditions**	**Surface Conditions**
CO_2	36.51 mM	15.34 mM
HCO_3^{-1}	99.94 mM	81.99 mM
CO_3^{-2}	0.03 mM	55.46 mM
OH^-	6.44x10^{-5} mM	0.15 mM
pH	6.79	10.16

References

1 Y. Hori, A. Murata and R. Takahashi, *J. Chem. Soc. Faraday Trans. 1*, 1989, **85**, 2309–2326.

2 M. Azuma, *J. Electrochem. Soc.*, 1990, **137**, 1772–1778.

3 F. Köleli, T. Atilan, N. Palamut, A. Gizir, R. Aydin and C. H. Hamann, *J. Appl. Electrochem.*, 2003, **33**, 447–450.

4 H. Li and C. Oloman, *J. Appl. Electrochem.*, 2005, **35**, 955–965.

5 K. P. Kuhl, E. R. Cave, D. N. Abram and T. F. Jaramillo, *Energy Environ. Sci.*, 2012, **5**, 7050–7059.

6 C. W. Li and M. W. Kanan, *J. Am. Chem. Soc.*, 2012, **134**, 7231–7234.

7 Q. Lu, J. Rosen, Y. Zhou, G. S. Hutchings, Y. C. Kimmel, J. G. Chen and F. Jiao, *Nat. Commun.*, 2014, **5**, 3242.

8 D. Kim, J. Resasco, Y. Yu, A. M. Asiri and P. Yang, *Nat. Commun.*, 2014, **5**, 4948.

9 K. Manthiram, B. J. Beberwyck and A. P. Alivisatos, *J. Am. Chem. Soc.*, 2014, **136**, 13319–25.

10 C. W. Li, J. Ciston and M. W. Kanan, *Nature*, 2014, **508**, 504–7.

11 S. Sen, D. Liu and G. T. R. Palmore, *ACS Catal.*, 2014, **4**, 3091–3095.

12 R. Kas, R. Kortlever, H. Yılmaz, M. T. M. Koper and G. Mul, *ChemElectroChem*, 2015, **2**, 354–358.

13 M. Ma, K. Djanashvili and W. a. Smith, *Phys. Chem. Chem. Phys.*, 2015.

14 E. L. Clark, M. R. Singh, Y. Kwon and A. T. Bell, *Anal. Chem.*, 2015, **87**, 8013–8020.

15 R. Kortlever, I. Peters, S. Koper and M. T. M. Koper, *ACS Catal.*, 2015, **5**, 3916–3923.

16 M. Sechenov, *Z. Phys. Chem*, 1889, **4**, 117.

17 A. Schumpe, *Chem. Eng. Sci.*, 1993, **48**, 153–158.

18 S. Weisenberger and A. Schumpe, *AIChE J.*, 1996, **42**, 298–300.

19 F. J. Millero, *Chem. Rev.*, 2007, **107**, 308–341.

20 L. N. Plummer and E. Busenberg, *Geochim. Cosmochim. Acta*, 1982, **46**, 1011–1040.

21 A. V. Bandura and S. N. Lvov, *J. Phys. Chem. Ref. Data*, 2006, **35**, 15.

22 Y.-G. Kim, J. H. Baricuatro, A. Javier, J. M. Gregoire and M. P. Soriaga, *Langmuir*, 2014, **30**, 15053–15056.

23 M. R. Singh, E. L. Clark and A. T. Bell, *Phys. Chem. Chem. Phys.*, 2015, **17**, 18924–18936.

24 N. Gupta, M. Gattrell and B. MacDougall, *J. Appl. Electrochem.*, 2006, **36**, 161–172.